ISSN 1063-7842, Technical Physics, 2019, Vol. 64, No. 12, pp. 1742–1748. © Pleiades Publishing, Ltd., 2019.
Russian Text © The Author(s), 2019, published in Zhurnal Tekhnicheskoi Fiziki, 2019, Vol. 64, No. 12, pp. 1836–1842.

23RD INTERNATIONAL SYMPOSIUM
"NANOPHYSICS AND NANOELECTRONICS,"
NIZHNY NOVGOROD, MARCH 11–14, 2019

Development of Technological Principles for Creating a System of Microfocus X-Ray Tubes Based on Silicon Field Emission Nanocathodes

N. A. Djuzhev[a], G. D. Demin[a,*], N. A. Filippov[a], I. D. Evsikov[a], P. Yu. Glagolev[a], M. A. Makhiboroda[a], N. I. Chkhalo[b], N. N. Salashchenko[b], S. V. Filippov[c], A. G. Kolosko[c], E. O. Popov[c], and V. A. Bespalov[a]

[a] *National Research University of Electronic Technology MIET, Zelenograd, Moscow, 124498 Russia*

[b] *Institute for Physics of Microstructures, Russian Academy of Sciences, Nizhny Novgorod, 607680 Russia*

[c] *Ioffe Institute, Russian Academy of Sciences, St. Petersburg, 194021 Russia*

** e-mail: gddemin@edu.miet.ru*

Received March 28, 2019; revised March 28, 2019; accepted April 15, 2019

Abstract—The technological prospects for the creation of a system of microfocus x-ray tubes with the use of silicon field emission of nanocathodes have been discussed. A numerical analysis of the field-emission current from a nanoscale semiconductor cathode regulated by voltage on a grid electrode has been carried out on the basis of which a scheme for controlling the elements of the matrix of field-emission cathode assemblies has been proposed. The current–voltage characteristics of silicon field emission nanocathodes have been measured. They are in good agreement with the theoretical estimates of the field-emission current. A full technological cycle of the development of elements of microfocus x-ray tubes (a set of field-emission cathode assemblies and a set of anode assemblies) has been performed. The results can be used to create systems of microfocus x-ray tubes for nanolithographic equipment of a new generation.

Keywords: field-emission, soft x-ray radiation, matrix of field-emission cathode assemblies, microfocus x-ray tube, silicon field nanocathodes

DOI: 10.1134/S1063784219120053

INTRODUCTION

Currently, there is an urgent need for miniature x-ray sources with low energy consumption, the ability to scan using an x-ray beam with a rapid adjustment of radiation frequency, as well as a short preparation time for use in various fields of science and technology. Such x-ray sources are in demand for a range of practical applications, such as medical equipment, x-ray fluorescence analysis equipment, security and counter-terrorism systems, etc. It is very attractive and promising in practical applications to use a field-emission cathode as an alternative to the traditional filament emitter in x-ray sources. A device based on a cold field-emission cathode provides better performance, a wider temperature range, and overall miniaturization. However, the main advantage of a nanoscale field-emission emitter in the context of x-ray sources is the narrow electron beam, which allows obtaining small focal spots on a target at sufficient intensity. Both a single field-emission cathode and a set of such emitters, which allows achieving high total values of the cathode current, can be used as an electron source depending on the specific application [1]. An additional step towards miniaturization of the x-ray source is the use of a through-type target combined with the output x-ray window [2]. Such a target structurally consists of a thin-film metal anode on a silicon membrane in which x-ray radiation is formed by an electron beam. The technology of microelectromechanical systems (MEMS) is the most promising for its formation, since it allows for reduction of the total cost and improves the manufacturability of the process of the production of x-ray windows. The idea of developing a set of microfocus x-ray tubes (MXRTs) based on the matrix of field emission cathode assemblies (FECAs), each of which consists of a tip-shaped silicon nanocathode controlled by a net-shaped electrode bus, is particularly attractive for x-ray lithography [3–5]. The practical implementation of such a concept requires both a serious technological study of the design of the FECA matrix based on MEMS technology and the electrical circuit of its control to create a topological pattern. This paper describes both theoretical and practical results obtained by our group in the development of a system of microfocus x-ray tubes using MEMS technology for the creation of silicon field-emission silicon nanocathodes.

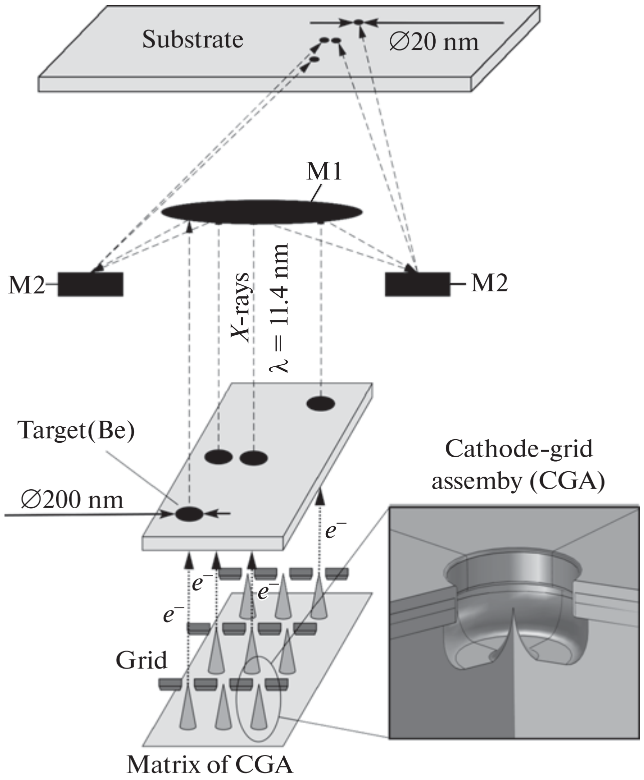

Fig. 1. Schematic representation of an MXRT system based on a controlled FECA matrix, where M1, M2, M3 are multilayer interference mirrors Mo(Ru)/Be.

1. THE CONCEPT AND TECHNOLOGY OF CREATING A MXRT SYSTEM BASED ON THE FECA MATRIX

A schematic representation of a MXRT system based on the matrix of silicon FECAs is presented in Fig. 1. The field-emission current from each element of the matrix (silicon field-emission nanocathode) is controlled by the blocking voltage on corresponding buses of net-shaped electrodes. The through-type target is made of an x-ray transparent beryllium membrane located on a thinned silicon plate 400 nm thick with a set of holes (anode assemblies). We have shown earlier in [6] that the choice of beryllium film thickness in the range from 100 to 200 nm allows obtaining the most efficient conversion of electronic energy into a soft x-ray radiation with a wavelength of 11.4 nm at an anode voltage of less than 4 kV. The MEMS x-ray optical system consisting of mirrors M1 and M2 based on multilayer structures Mo(Ru)/Be with a high reflection coefficient (more than 70%) allows for improvement of the resolution of x-ray radiation coming out of the through-type target by almost 10 times, which opens the way to reduce the diameter of the x-ray beam to 20 nm and below [7].

1.1 The Description of the Technology of the FECA Matrix Formation

The FECA matrix in the MXRT system is needed for ignition of a predetermined sequence of single pixels by turning on/off the field-emission current from selected autocathodes. Each element of the FECA matrix is responsible for the formation of a single pixel of the topological pattern on the substrate in relation to problems of x-ray nanolithography. It is supposed to include individual elements from the FECA matrix at the construction of topological patterns of various kinds, while the rest of the elements remain in the off state. An array of nanoscale tip-shaped autocathodes, controlled by the buses of net-shaped electrodes included in the FECA, was manufactured in the following way. Silicon plates phosphorus-doped with (100) orientation and a diameter of 150 mm were oxidized in oxygen with water vapor (the thickness of the SiO_2 forming layer was 0.3 μm), a Si_3N_4 layer was then deposited on them as a mask with a thickness of 0.1 μm, after which photolithography was carried out to form T-shaped columns as blanks for silicon nanotips. The tip profile was formed using plasma chemical etching in a mixture of SF_6 and O_2 with an anisotropy coefficient of 2.5. The cathode oxidation procedure was carried out in dry oxygen, after which SiO_2 was etched off together with the mask layer. Two photos of field-emission structures obtained as a result of the above-described technological operations are presented in Fig. 2: an array of nanoscale silicon tips with a nanometer radius of rounding at the top and a FECA based on them with a controlling net bus.

1.2. Description of the Technology of Forming a Matrix of Anode Assemblies

The matrix of anode assemblies as part of the MXRT system is designed to generate x-ray radiation in the holes of a through-type target located opposite "turned on" FECAs with a spatial resolution corresponding to their diameter. For this purpose, a thinned silicon plate with a thickness of 400 nm is oxidized, a TiN film with a thickness of 20 nm is then deposited on SiO_2 as a protective layer that prevents the etching of the beryllium membrane during subsequent removal of SiO_2 and polysilicon (Si*) etching operations. A 200-nm-thick beryllium layer is then deposited on the plate, followed by a 30-nm-thick TiN layer deposited on it, on top of which 450 nm of Si* is deposited. Next, polysilicon photolithography is carried out. The Bosch Process etches wide depressions with a cross-sectional diameter of about 400 nm on the reverse side (see insert in Fig. 3) in places located opposite silicon nanocathodes on the front side of the plate up to the SiO_2 layer. The silicon residues on the membrane (micrograss) are further removed in XeF_2, liquid chemical etching of SiO_2 is performed, and the

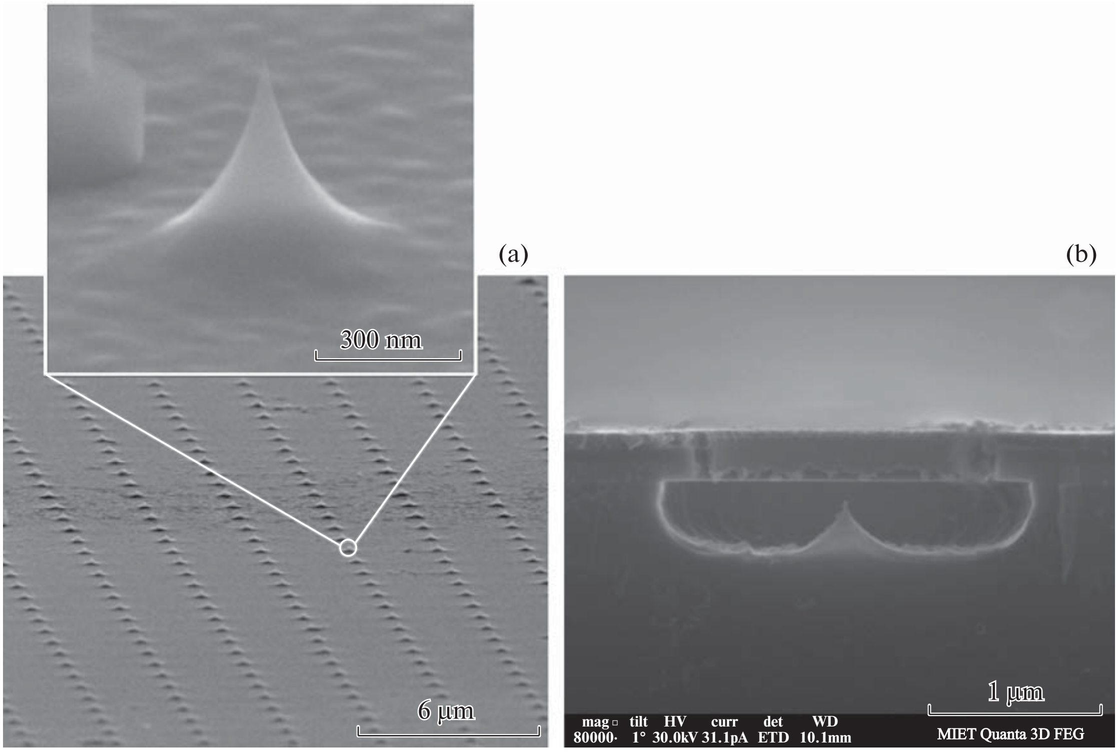

Fig. 2. Images of (a) a matrix of silicon field-emission nanocathodes and (b) a cross section of FECAs based on them, obtained by SEM.

protective layers of TiN are etched off to form the final structure of the anode assemblies matrix. The image of the workpiece for the matrix of anode assemblies before the deposition of the beryllium layer is shown in Fig. 3. It is assumed that the choice of a beryllium membrane thickness of 200 nm provides its improved mechanical and thermal properties.

1.3. Description of the MXRT System Assembly Process

The following conditions should be met for the correct operation of the MXRT system at the alignment of the FECA matrix and the matrix of anode assemblies: (1) the accuracy of the alignment should be at least 1 μm; (2) there should be no conductivity between the anode and cathode parts; (3) the distance between the cathode and anode parts should be about 10 μm. The process of splicing plates with a Brewer-BOND® 305 intermediate layer is best suited to achieve this task. The technology of combining the FECA matrix and the matrix of anode assemblies includes the following steps: a preparation of the plate with the FECA matrix; applying a layer of Brewer-BOND® 305 with a thickness of 10–15 μm on a plate with the FECA matrix; photolithography of the plate with the FECA matrix over the applied intermediate layer; preparation of the plate with the matrix of anode assemblies; and combining the plates with the FECA matrix and the matrix of anode assemblies in the installation for splicing plates. The MXRT system, presented in Fig. 4, is obtained as a result of operations.

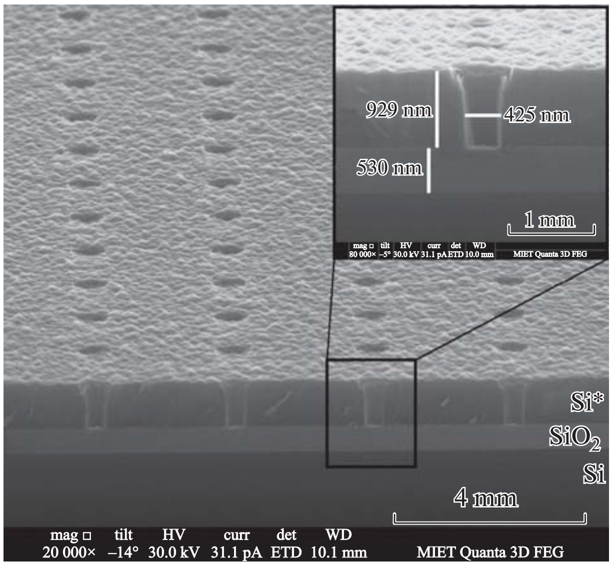

Fig. 3. Image of a workpiece for the matrix of anode assemblies before sputtering a through-type target (Be), consisting of an x-ray transparent membrane (Si/SiO_2) and a layer of polysilicon (Si∗) with a set of holes, obtained by SEM.

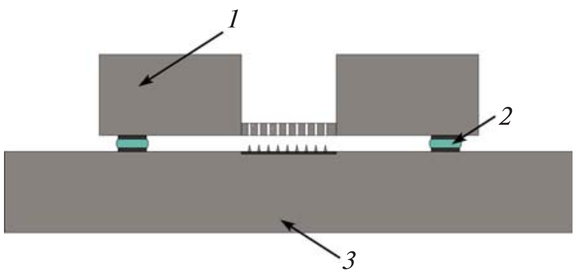

Fig. 4. The MXRT system obtained by gluing the FECA matrix and the matrix of anode assemblies, where (*1*) is the matrix of anode assemblies, (*2*) is solder, and (*3*) is the FECA matrix.

1.4. Control Circuit of the FECA Matrix Elements

Earlier, we presented a quantum-mechanical model for calculating the current of field-emission from a nanoscale semiconductor cathode of arbitrary shape considering its thermal heating by an electric field [8], which allowed the partial explanation of the difference between the experimentally measured field-emission currents and their theoretical values obtained in the framework of the Fowler–Nordheim theory [9]. According to the Tsong model [10], the bending of zones $V_S(x, y, z) = -\phi_S(x, y, z)/e$, which is due to the penetration of an electric field into the near-surface layer of a silicon emitter with n-type doping, is determined by the solution of Poisson equation

$$\frac{d^2\eta_\varphi}{dr_\delta^2} + \frac{2}{r_\delta}\frac{d\eta_\varphi}{dr_\delta} = f(\eta_\varphi, N_a, N_d), \quad (1)$$

where potential energy, $\eta_\varphi = \phi_S/k_BT$, $r_\delta = r/\delta$, $r = \sqrt{x^2 + y^2 + z^2}$, $\delta = (\zeta\varepsilon_0 k_B T/2n_i e^2)^{1/2}$ is the depth of the Debye screening in silicon, ζ is the silicon dielectric constant, ε_0 is a permittivity, k_B is the Boltzmann constant, T is the emitter heating temperature, e is the electron charge, and n_i is the electron (hole) concentration in the intrinsic semiconductor. On the right side of Eq. (1), function $f(\eta_\varphi, N_a, N_d) = [\Phi(\eta_\varphi^2, \eta_\varphi, \varphi_\varepsilon^F, \varphi_\varepsilon^v)]$ in the case of total ionization of impurities, where $N_{a(d)}$ is the concentration of the acceptor (donor) impurity, $\eta_\varepsilon^F = \varepsilon_F/k_BT$, $\eta_\varepsilon^{v(c)} = \varepsilon_{v(c)}$, $\eta_\varphi^B = \sinh^{-1}((N_a - N_d)/2n_i) = \varphi_B/k_BT$, $\varphi_B = \varepsilon_{Fi} - \varepsilon_F$, ε_{Fi} is the Fermi level in the intrinsic semiconductor, ε_F is the Fermi level, $\varepsilon_{v(c)}$ is the bottom of the valence band (the conduction band), and $\Phi = \Phi(\eta_\varphi^B, \eta_\varphi, \eta_\varphi^2, \eta_\varphi^v, \eta_{\varphi^c})$ is the function calculated through the Fermi integrals of the 1/2 order. When calculating Eq. (1), boundary condition $d\eta_\varphi/dr_\delta\ (r_\delta \to -\infty) = 0$ is used.

It is worth considering that the heating of the silicon nanocathode in the flow of the emission current is taken into account through the implementation of boundary conditions on the surface of the silicon emitter [11]:

$$J = \delta\nabla V_s \cdot \mathbf{e}_\mathrm{n}, \quad (2)$$

where $\sigma = \sigma(x, y, z, T)$ is the temperature- and size-dependent conductivity of the emitter, $\mathbf{e}_\mathrm{n}$ is the unit vector perpendicular to the surface of the emitter, which is calculated from Eq. (1) via the parameter η_φ, and the emission current density in Eq. (2) is determined by the Fowler–Nordheim equation [12]:

$$J = \frac{A_0 E^{2-v}}{\phi t_0^2}\left(\frac{\phi^2 \exp(6)}{4Q}\right)^v \exp\left(-B_0\frac{\phi^{3/2}}{E}\right), \quad (3)$$

where $A_0 = e/16\pi^2\hbar$, $B_0(4/3\hbar)\sqrt{2m_e}$, $v = 2B_0Q/3\sqrt{\phi}$, m_e is the electron mass, $\hbar$ is the Planck constant, $Q = e^2/16\pi\varepsilon_0$, $t_0 = 1 + 1/(6\exp(1))$, and E is the electric field on the surface of the emitter. When integrating Eq. (3) over the entire effective emission area of S_eff, the current is obtained, i.e., $I = \int J\,dS \approx JS_\mathrm{eff}$. The volt–ampere characteristics (VAC) taken from a single silicon nanocathode in diode mode is shown in Fig. 5. It was theoretically calculated by Eq. (3) for the case of the interelectrode distance equal to 10 μm at the cathode voltage of 30 V and anode voltage of 3 kV. Assuming that the current is switched on at an electric field of the order $E = E_\mathrm{cr}$ = 3–3.1 V/nm, the threshold control voltages on the net that are necessary to turn on/off the emission current in the FECA matrix element, whose geometric dimensions are taken in accordance with Fig. 2 (where the SEM image of its cross-section is presented), were evaluated on the basis of the presented model and a schematic and topological library of the elements for reading the electrical signal was developed. It is clearly seen from Fig. 5 that the E_cr value is achieved at a net voltage of about 15 V. Table 1 illustrates the switching scheme of the i–j-elements of the FECA matrix, which is necessary for the ignition of a given configuration of pixels of the topological pattern formed on the substrate playing the role of the anode using the MXRT system. The variation of the voltage at the ith bus of the net-shaped electrode from 0 to 15 V includes a separate i–j-element of the FECA in the matrix when the voltage on jth cathode bus is 30 V, while the rest of the cathode bus voltages are –30 V. Wherein, the through-type target (anode) voltage is set to 3 kV. In this case, when the distance from the cathode to the anode is fixed at 10 μm, the characteristic size of the spot from a single nanocathode on the target is about 2 μm, which covers the spatial region of x-ray beam generation at the location of the hole in the x-ray transparent membrane (Fig. 3).

2. EXPERIMENTAL TECHNIQUE

The measurement of field-emission characteristics of the cathode part of the device (the plate with the FECA matrix) was carried out using a multichannel computerized installation with a high-voltage vacuum station [13].

During installation, a semi-sinusoidal voltage pulse from a pulse source with a frequency of 50 Hz (i.e., a half-period is a negative pulse in terms of a sinusoidal voltage and half a period has a zero voltage) is applied to a sample and the profile of the corresponding field-emission current pulse is then recorded, which allows the recording of the VAC from the FECA matrix every 20 ms. This approach makes it possible to obtain characteristics of increased smoothness that differ from those obtained at the mode of the slow scan by constant voltage. The relationship between fast and slow VACs was studied earlier in [14]. A high speed of a VAC recording in conjunction with the developed methodology of data online processing provides the ability to calculate not only cathode effective characteristics (the amplification factor of the field β_{eff} and emission area S_{eff}), but also their stochastic dispersion, which characterizes the degree of VAC variability and is one of the causes of temporary instability of the emission current. The effective parameters are calculated by the known method of constructing a straight trend line to the VAC in semi-logarithmic Fowler–Nordheim coordinates. The equation of field-emission in the Elinson–Schrednik annotation [15], reduced to macroscopic values of current I and voltage U and written in SI units: $I = S_{eff}A_{\phi}(U\beta_{eff}/d)\exp(-B_{\phi}d/U\beta_{eff})$, where the corresponding variables in the current formula $A_{\phi} = 1.4 \times 10^{-6}\, A \cdot eV \cdot V^2]\exp(10.17/\phi^{1/2})/\phi$, $B_{\phi} = 6.49 \times 10^9[eV^{-3/2} \cdot V/m]\, \phi^{3/2}$, ϕ is the work function of emitter material, and d is the interelectrode distance, is used to derive the relationship of the effective parameters β_{eff} and S_{eff} with slope (K) and cutoff (S) of the trend line. This equation takes the following form in semi-logarithmic coordinates: $\ln(I/U^2) = \ln(\beta^2_{eff}A_{\phi}S_{eff}/d^2)B_{\phi}d/U\beta_{eff} = S + K/U$. Then, the effective parameters can be calculated by the following formulas:

$$\beta_{eff} = B_{\phi}d/K, \quad S_{eff} = \exp(S)d^2/A_{\phi}\beta^2_{eff}. \tag{4}$$

3. EXPERIMENTAL RESULTS

The construction of the experimental VAC in semi-logarithmic Fowler–Nordheim coordinates and its approximation by a straight-line correlation allow the calculation of the values of the effective parameters: the field gain coefficient and emission area. These are the two main parameters that characterize the efficiency of a field-emission nanocathode. The experimental VAC in normal and in Fowler–Nordheim coordinates and model curves approximating them are shown in Fig. 6. These results were obtained at an interelectrode distance of 300 μm under technical vacuum conditions (10^{-5} Pa). The choice of such a distance in the experiment is necessary to prevent high currents and overheating at the anode. It is easy to see from the figure that the FECA matrix allows for obtaining a field-emission current of more than 100 μA at an anode voltage of 3 kV and above. It is assumed that an x-ray radiation with a conversion coefficient on the order of 10^{-4}, the calculations of which were carried out earlier in [6], will be formed in the matrix of anode assemblies at such a voltage and current. The evaluation of effective field amplification factor β_{eff} and emission area S_{eff} in accordance with Eq. (4) gave the following results: $\beta_{eff} = 250$ (in dimensionless units) and S_{eff} = 340 nm^2. The value has an order of magnitude characteristic of nanocathodes of this kind. It characterizes the increase in the field at the top of the cathode due to its form-factor.

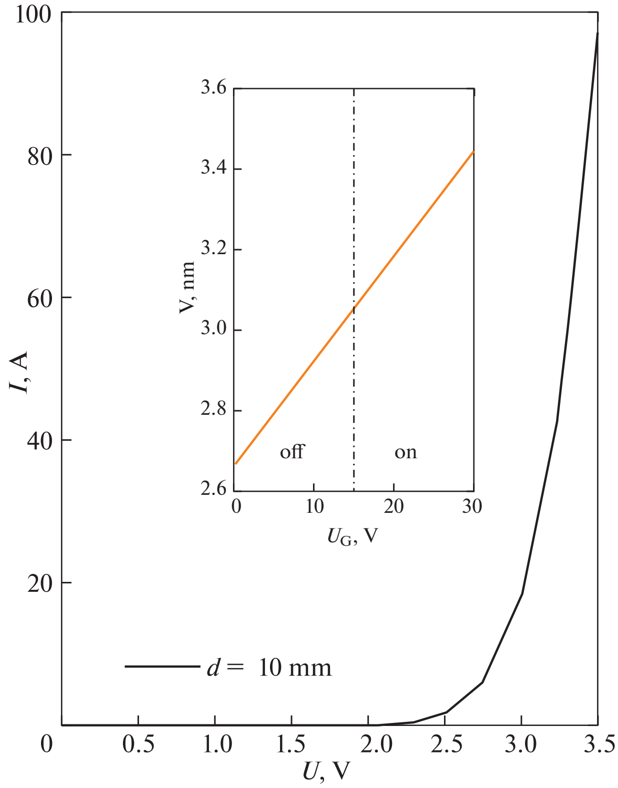

Fig. 5. VAC from a single silicon nanocathode, calculated by Eq. (3) at an interelectrode distance of 10 μm and anode voltage of 3 kV. The inset shows the dependence of the electric field strength at the top of the nanocathode on the voltage at the net-shaped electrode at the same parameters.

Table 1. The scheme for switching the state of the elements of the FECA matrix (at a voltage on the target of 3 kV)

The state of the i–jth element of the FECA matrix	Off	On
Selected ith net bus (V)	0	15
Selected jth cathode bus (V)	30	
Other net buses (V)	0	
Other cathode buses (V)	30	–30

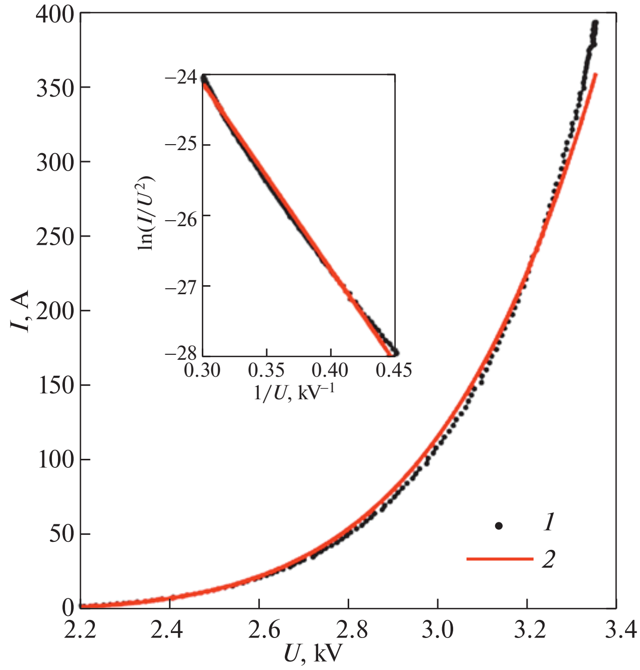

Fig. 6. VAC taken from the matrix of silicon field-emission nanocathodes, in the usual and Fowler–Nordheim coordinates (see inset), where (*1*) are experimental curves and (*2*) are approximating curves constructed using effective parameters.

CONCLUSIONS

Thus, the main technological principles of creating the MXRT system on the basis of combining the FECA matrix based on silicon field-emission nanocathodes and the matrix of anode assemblies as an integral part of the through-type target was considered in detail in this study. The results of technological implementation of individual elements of the MXRT system, in particular, the FECA matrix and matrix of anode assemblies, using basic operations of silicon MEMS technology are presented. The technique of reading the VAC from the matrix of silicon tip-shaped autocathodes, designed to record the measured signals and subsequent processing of received data on their emission properties in real time was described. It was shown that a current of 100 βA is collected from the matrix of nanoscale silicon emitters when the voltage is about 3 kV in the field-emission mode. As shown in [6], the power density on the matrix of anode assemblies corresponding to such a value of the emission current will exceed 1 W/cm^2, which is sufficient for effective conversion of the energy of electrons into a soft x-ray radiation. The next step in the development of the MXRT system based on the FECA matrix is to find the optimal parameters of an x-ray generation in the matrix of anode assemblies. The use of these technological solutions to create elements of the MXRT system in conjunction with the use of high-performance x-ray optics opens the way to the development of an x-ray nanolithography to create structures with a size of up to 20 nm and below [16].

FUNDING

The work was performed by a group of authors, which includes N.A. Djuzhev, G.D. Demin, N.A. Filippov, I.D. Evsikov, P.Yu. Glagolev, M.A. Makhiboroda, N.I. Chkhalo, and N.N. Salashchenko, who used the equipment of the Collective Use Center Microsystem Technology and Electronic Component Base, National Research University of Electronic Technology, supported by the Ministry of Education and Science of Russia as part of project 14.578.21.0250, RFMEFI57817X0250 using the Center for National Technology Initiative Sensory.

CONFLICTS OF INTEREST

The authors state that they do not have any conflicts of interest.

REFERENCES

1. S. A. Guerrera and A. I. Akinwande, Nanotechnology **27**, 295302 (2016). https://doi.org/10.1088/0957-4484/27/29/295302
2. S. F. Wang, H. Y. Chiang, Y. J. Liao, R. S. Liu, C. C. Cheng, H. W. Yang, S. W. Wang, Y. C. Lin, and S. M. Hsu, Radiat. Phys. Chem. **158**, 188 (2019). https://doi.org/10.1016/j.radphyschem.2019.02.005
3. G. D. Demin, N. A. Djuzhev, N. A. Filippov, P. Yu. Glagolev, I. D. Evsikov, and N. N. Patyukov, J. Vac. Sci. Technol. B **37**, 022903 (2019). https://doi.org/10.1116/1.5068688
4. N. A. Djuzhev, G. D. Demin, T. A. Gryazneva, A. E. Pestov, N. N. Salashchenko, N. I. Chkhalo, and F. A. Pudonin, Bull. Lebedev Phys. Inst. **45**, 1 (2018). https://doi.org/10.3103/S1068335618010013
5. N. N. Salashchenko, N. I. Chkhalo, and N. A. Djuzhev, J. Surf. Invest.: X-Ray, Synchrotron Neutron Tech. **10**, 10 (2018). https://doi.org/10.1134/S1027451018050324
6. A. Ya. Lopatin, D. E. Par'ev, A. E. Pestov, N. N. Salashchenko, N. I. Chkhalo, G. D. Demin, N. A. Dyuzhev, M. A. Makhiboroda, and A. A. Kochetkov, J. Exp. Theor. Phys. **127**, 985 (2018). https://doi.org/10.1134/S1063776118100175
7. N. I. Chkhalo and N. N. Salashchenko, AIP Adv. **3**, 082130 (2013). https://doi.org/10.1063/1.4820354
8. N. A. Djuzhev, G. D. Demin, P. Yu. Glagolev, M. A. Makhiboroda, and N. N. Patyukov, *Proc. 31st Int. Vacuum Nanoelectronics Conf., Kyoto, Japan, 2018*, p. 116. https://doi.org/10.1109/IVNC.2018.8520046
9. R. G. Forbes, *Proc. 31st Int. Vacuum Nanoelectronics Conf., Kyoto, Japan, 2018*, p. 126. https://doi.org/10.1109/IVNC.2018.8520077
10. T. T. Tsong, Surf. Sci. **85**, 1 (1979). https://doi.org/10.1016/0039-6028(79)90228-0

11. K. Eimre, A. Aabloo, F. Djurabekova, and V. Zadin, J. Appl. Phys. **118**, 033303 (2015). https://doi.org/10.1063/1.4926490
12. K. L. Jensen, *Introduction to the Physics of Electron Emission* (Wiley, 2018).
13. E. O. Popov, A. G. Kolosko, S. V. Filippov, P. A. Romanov, and I. L. Fedichkin, Mater. Today: Proc. **5**, 13800 (2018). https://doi.org/10.1016/j.matpr.2018.02.021
14. E. O. Popov, A. G. Kolosko, S. V. Filippov, P. A. Romanov, E. I. Terukov, A. V. Shchegolkov, and A. G. Tkachev, Appl. Surf. Sci. **424**, 239 (2017). https://doi.org/10.1016/j.apsusc.2017.04.120
15. *Cold Cathodes*, Ed. by M. I. Elinson (Sov. Radio, Moscow, 1974).
16. J. R. Maldonado and M. Peckerar, Microelectron. Eng. **161**, 87 (2016). https://doi.org/10.1016/j.mee.2016.03.052

Translated by N. Petrov

SPELL; OK